CHAPTER 7

PROPOSED MODEL OF THE HOLLOW CATHODE HELIUM-CADMIUM AFTERGLOW

7.1 INTRODUCTION

To obtain further confirmation of the dominant role of the Penning collision mechanism in populating the $5s^2\ ^2D_{5/2}$ level of Cd II in a $He\text{-}Cd^+$ hollow cathode discharge, the afterglow of the discharge was investigated. The study consisted initially of an investigation of the decay of the 4416 Å spontaneous emission and the results were presented and discussed in Chapter 4. In Chapter 5 the mechanism leading to the excitation of the $5s^2\ ^2D_{5/2}$ level late in the afterglow was unambiguously shown to be that of Penning type collisions between cadmium neutral and helium 2^3S metastable atoms. The early afterglow characteristics of the 4416 Å decay, in particular, the intensity increase and subsequent rapid decay, could not be readily explained by the model proposed in Chapter 5 (viz $5s^2\ ^2D_{5/2}$ excitation by Penning collisions and 2^3S decay by Penning collisions and diffusion) and some investigation of this region was essential if the afterglow data is to be extrapolated back to conditions prevailing in the d.c. discharge.

In Chapter 6 mechanisms which were thought to play an important role in the early afterglow were proposed and their significance assessed. On the basis of this investigation it was postulated that the Penning collision mechanism is solely responsible for populating the upper level of the 4416 Å Cd II laser transition in the afterglow and that the observed variations in the 4416 Å intensity reflect the changes in the

2^3S density. Additional processes directly influencing the 2^3S population in the early afterglow were proposed to be those of metastable production via electron collisional de-excitation and radiative decay of the higher lying helium levels and 2^3S destruction via conversion to the ground state by collisions of the second kind. These additional electronic processes were shown to be significant in the early afterglow where the electron density is high and the electron temperature low as the hollow cathode discharge has a predominance of thermalized electrons.

Because of experimental difficulties it was not possible to assess the validity of this model through direct measurement of the temporal evolution of the He (2^3S) population in the early afterglow. Investigation of the proposed mechanism is therefore confined to that of modelling the afterglow, incorporating the collision processes discussed in Chapter 6, and evaluating the accuracy of the model using the steady state electron, ion and excited state densities reported in Chapter 3 along with estimates for the electron energy distribution function and collision cross section data for the processes considered. This chapter reports the development of and results predicted by the model.

This chapter begins (section 7.2) with a discussion of the rate equations of the important excited state and ionic ground state densities of helium, the electron density and electron and gas temperatures. Initially, all collision processes are included and the rate equations later simplified by the elimination of those mechanisms either known or shown to be insignificant in the afterglow of the hollow cathode discharge.

As discussed in section 7.3 the model quantitatively accounts for the experimental observations of the 4416 Å spontaneous decay. Indeed, the parametric variation of the decay with current, pressure and cadmium

concentration (reported in Chapter 4), are easily explained. The observed intensity increase is a result of an increase in the 2^3S density in the early afterglow through the efficient and rapid conversion of the higher lying levels, including the 2^1S level, to the triplet metastable via radiative decay and electron collisional relaxation. Thus production of the 2^3S species is maintained in the early afterglow whereas the overall losses are greatly reduced as the process of electron impact ionization (the dominant loss mechanism for the 2^3S species in the steady state discharge) is no longer energetically possible. Further, the initial losses of the 2^3S population are due not only to Penning collisions and diffusion but also electronic de-excitation to the ground state, with this latter process becoming less significant as the electron density decays in the late afterglow. Thus the decay of the 2^3S population, and hence 4416 Å spontaneous emission, is more rapid in the early afterglow than if Penning collisions and diffusion alone were active.

The current and pressure dependence of the point of intersection of the extrapolated exponential tail (reported in section 4.5.2 and 4.5.3) is then explained by the increased importance of electronic de-excitation of the 2^3S level as the electron density is a monotonically increasing function of these two parameters. The current and pressure dependence of the relative peak height, also reported in section 4.5.2 and 4.5.3, are explained by the parametric variation of the 2^3S, 2^1S, 2^3P and 2^1P densities. With increasing current the 2^3S density increases monotonically whereas the density of the other helium levels remains constant and thus, conversion of the latter to the former results in a smaller percentage increase in the population of the triplet state.

Similarly, results presented in Chapter 3 show that, with increasing pressure, the relative densities of all excited state helium atoms remain constant and thus the relative peak heights will also remain constant.

Throughout the discussion it is assumed that the $5s^2\ ^2D_{5/2}$ level of the cadmium ion decays predominantly by spontaneous emission to the $5p\ ^2P_{3/2}$ level, however, because of the high electron densities and low temperatures in the afterglow electronic relaxation of this level must also be considered. In section 7.4 the role of electron collisional de-excitation of the $5s^2\ ^2D_{5/2}$ level is considered. While it is difficult to accurately assess the importance of this process it is argued that, even if this process were significant and were to be included in the decay of this level it would not affect the qualitative discussion of section 7.3 or the quantitative development of section 7.5.

In section 7.5 the system of simplified rate equations developed in section 7.2 is solved and the results of these calculations are compared with the decay of the 4416 Å spontaneous emission. Using estimates for the electron energy distribution function and the best available data for the collision cross sections along with the initial excited state, electron and ion densities presented in Chapter 3, the model clearly predicts that the 2^3S metastable density could indeed have a temporal evolution in the afterglow identical to the decay of the 4416 Å spontaneous emission. Further, the current, pressure and oven temperature dependence of the decay are also reproduced.

In a final attempt to verify experimentally the proposed mechanism, section 7.6 reports the results of an experiment whereby the 3889 Å intensity regrowth curve was recorded with a high temporal resolution (RC limitation < 1 μsec). The data obtained was not of sufficient quality to analyse with any degree of confidence; however, the evolution of the

intensity regrowth curve suggests that the He (2^3S) density does indeed increase early in the afterglow.

7.2 DEVELOPMENT OF THE RATE EQUATIONS

7.2.1 Decay of the Helium 2^3S Metastable Density

In the afterglow the helium 2^3S metastable atoms are destroyed by Penning collisions, metastable-metastable interactions and electron de-excitation to the helium ground state. Early in the afterglow production of the metastable species occurs via relaxation of the higher lying helium levels and, less significantly, by recombination. Thus the rate equation governing the evolution of the 2^3S metastable density is

$$\frac{dN(2^3S)}{dt} = -n_e(N(2^3S)\ R_{de\text{-}ex} - N(2^3S)\ N_{Cd} < \sigma_p v > - \frac{D_m\ N(2^3S)}{\Lambda^2 p}$$

$$- \delta[N(2^3S)]^2 + \sum_i n_e N_i R^i_{conv} + \sum_i A_i N_i + k\alpha n_e N(He^+) \qquad (7.1)$$

where n_e, $N(He^+)$, $N(2^3S)$ and N_i are all functions of time and represent the electron, ion, 2^3S metastable and excited helium densities (with energies greater than the triplet metastable) respectively. $N_{Cd} < \sigma_p v >$, $R_{de\text{-}ex}$ and $D_m/\Lambda^2 p$ are the Penning, electron de-excitation and diffusion rate coefficients. The two terms $\sum_i n_e N_i R^i_{conv}$ and $\sum_i A_i N_i$ represent metastable production through electron knockdown from higher lying levels i (rate coefficient R^i_{conv}) and radiative decay into the metastable level from those states optically connected to it.

Although the molecular metastable and ion species could provide additional production mechanisms for the atomic metastable species, Gill

(1975) has shown that the expected densities of the molecular species are small ($\sim 10^9$ cm^{-3}) and these processes can be neglected from the discussion of the afterglow. A study of the spectra from the present discharge tube revealed nothing to invalidate this assumption. Destruction of the 2^3S metastable atoms through conversion to an excited molecular state is also not considered because of the small rates of the conversion mechanisms (Deloche et al., 1976).

Although the rate coefficient for metastable-metastable ionization is relatively large ($\delta = 1.5 \times 10^{-9}$ cm^3 sec^{-1}; Deloche et al., 1976) the low metastable densities ($\sim 10^{12}$ cm^{-3}) make this process less significant than loss via Penning collisions and electron knockdown. Also, recombination has been shown (Chapter 6) to be an insignificant production mechanism in the helium-cadmium afterglow.

Thus equation (7.1) can be simplified to

$$\frac{dN(2^3S)}{dt} = -n_e(N(2^3S)\ R_{de\text{-}ex} - N(2^3S)\ N(Cd) < \sigma_p v >$$

$$- \frac{D_m N(2^3S)}{\Lambda^2 p} + \sum_i N_i A_i + \sum_i n_e N_i R^i_{conv} \qquad (7.2)$$

The only levels, other than the 2^3S, with significant populations are the 2^1S, 2^1P and 2^3P levels and only these will be considered in the triplet metastable production terms ($\sum_i N_i A_i + \sum_i n_e N_i R^i_{conv}$) of equation (7.2).

7.2.2 Decay of the Higher Lying Helium Levels

The rate equation governing the decay of the higher lying levels

(N_i) of helium can be written as

$$\frac{dN_i}{dt} = -n_e N_i R^i_{de\text{-}ex} - n_e N_i R^i_{conv} - N_i N_{Cd} \langle \sigma^i_p v \rangle - A^T_i N_i - \frac{D_i N_i}{\Lambda^2_p} + k_i \alpha n_e N(He^+) \quad (7.3)$$

where the loss terms represent electron de-excitation to the ground state, conversion to the 2^3S level, Penning collisions, radiative decay (to all levels at a rate A^T_i) and diffusion. Production due to recombination is included.

Because conversion to the 2^3S level proceeds more rapidly than diffusion and de-excitation to the helium ground state (the cross section for de-excitation is approximately two orders of magnitude less than for conversion to the 2^3S level; Fujimoto, 1978) equation (7.3) can be simplified to

$$\frac{dN_i}{dt} = -n_e N_i R^i_{conv} - N_i N_{Cd} \langle \sigma_p v \rangle - A^T_i N_i \quad (7.4)$$

Recombination has again been deleted from this rate equation. The Penning collision term, although not a significant loss mechanism at low oven temperatures, is important at higher oven temperatures and must be included in the simplified rate equation.

7.2.3 Decay of the Helium Ions

In the afterglow the helium ions will be destroyed by thermal charge transfer collisions with cadmium, diffusion to the walls and recombination. Production of the helium ions occurs via metastable-

metastable ionization. Thus, the helium ion rate equation can be written as

$$\frac{dN(He^+)}{dt} = D_1\nabla\left[\left(1 + \frac{T_e}{T_g}\right)\nabla N(He^+)\right] - N(He^+)\, N_{Cd} < \sigma_{TH} v > - \alpha n_e N(He^+) + \delta [N(2^3S)]^2 \qquad (7.5)$$

where the first term represents the loss through diffusion with coefficient D_1 (in $cm^2\ sec^{-1}$), the second and third terms loss through collisions with cadmium (with a rate $\langle\sigma_{TH}\bar{v}\rangle$ where σ_{TH} is the thermal energy charge transfer collision cross section) and recombination respectively and the last term the production due to metastable-metastable interactions.

Treating the diffusion term alone, and assuming that the discharge is symmetric in all but the radial coordinate, it can be shown that diffusion plays a minor role in the loss processes of the helium ion. As discussed above, production through metastable-metastable ionization provides a negligible contribution to the ion density and the experimental evidence of Chapter 6 shows that, when compared with thermal energy charge transfer, recombination plays a minor role in depopulating the helium ion species. Thus, the decay of the helium ion density can simply be written as

$$\frac{dN(He^+)}{dt} = -N(He^+)\, N_{Cd} < \sigma_{TH} v > \qquad (7.6)$$

7.2.4 Decay of the Electron Density

Charge neutrality requires that

$$n_e = N(He^+) + N(Cd^+) \qquad (7.7)$$

where $N(Cd^+)$ is the total cadmium ion density.

Results of the absorption experiment (Chapter 3) have shown that

$$N(Cd^+) \ll N(He^+) \qquad (7.8)$$

in the steady state, but because thermal charge transfer and Penning ionization result in the formation of an excited cadmium ion it is possible that the ion density could increase to an appreciable fraction of the helium ion density in the early afterglow, and the above condition might no longer be valid.

To investigate this, the cadmium ion ground state density decay was determined from the line absorption at 2144 Å ($5p\ ^2P_{3/2} - 5s\ ^2S_{1/2}$) using the method described in Chapter 5. Results, showing the intensity regrowth and spontaneous decay at 2144 Å, are given in Figures 7.1a - 7.1b. The corresponding ion decay, plotted on a semi-logarithmic scale, is shown in Figure 7.1c. For all experimental conditions the ion density decays exponentially in the late afterglow indicating that diffusion is the only significant loss mechanism at these times. Using a method similar to that discussed in section 4.5.3, in which the decay is

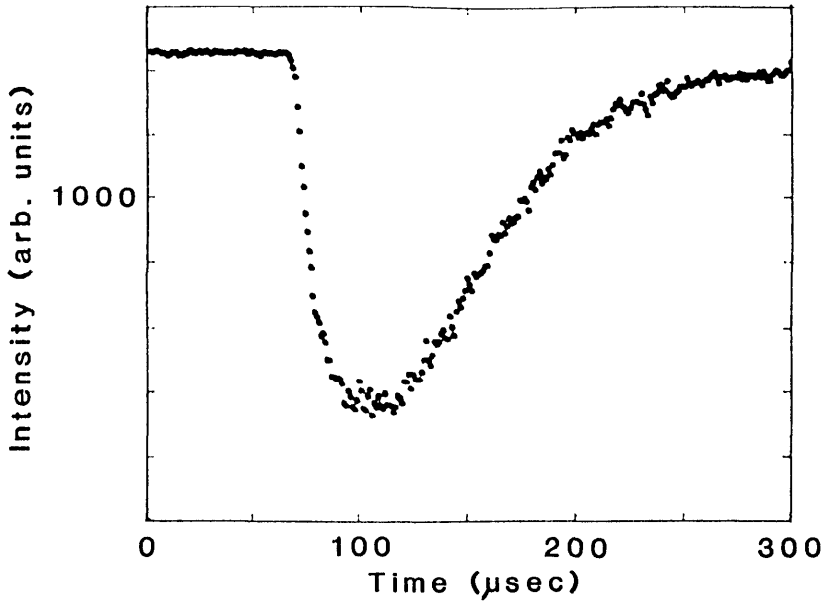

Figure 7.1a
Intensity regrowth curve at 2144 Å for an oven temperature of 250^{0}C, 120 mA/anode and a pressure of 20 Torr

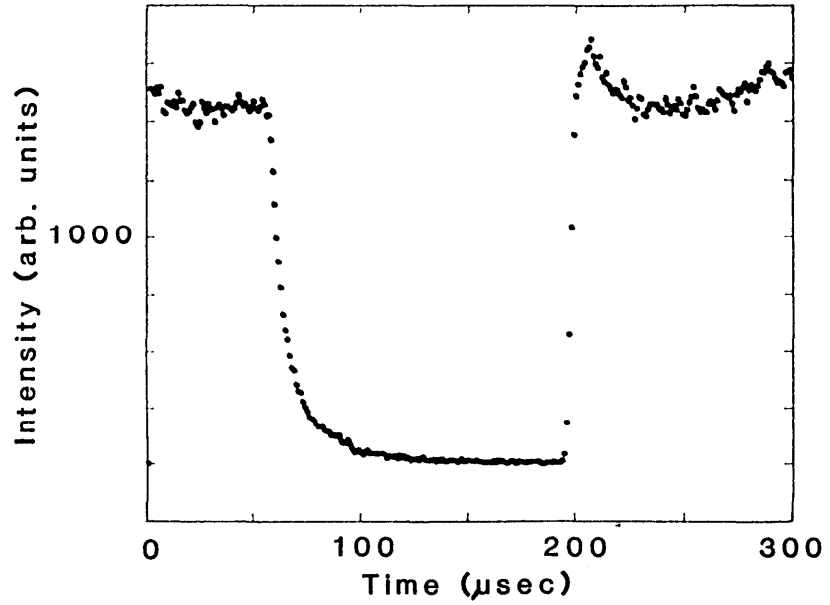

Figure 7.1b
Decay of the Cd II 2144 Å spontaneous emission at an oven temperature of 250^{0}C, 120 mA/anode and a pressure of 20 Torr

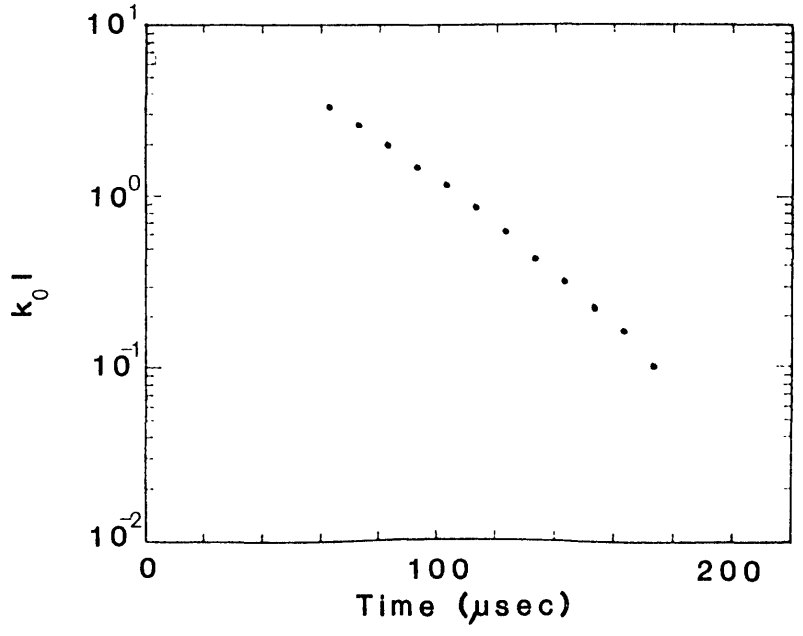

Figure 7.1c
Semi-logarithmic plot of the cadmium ion density ($k_0 l$) versus time after current termination. Conditions as for Figure 7.1a

measured as a function of gas pressure, the diffusion coefficient for the cadmium ions was calculated to be

$$D_+ = 545 \pm 100 \ cm^2 \ torr^{-1} \ sec^{-1}$$

Because of the long lived spontaneous decay at 2144 Å (Figure 7.1b) no experimental information concerning the evolution of the cadmium ions for times less than ∿55 μsec could be obtained.

To bridge the gap between the known value at T=0 and the observed decays for t > 55 μsec the recombination coefficient in the rate equation for the cadmium ions was adjusted so that it adequately represented the experimental results. The rate equation can be written as

$$\frac{dN(Cd^+)}{dt} = N(He^+) \ N_{Cd} < \sigma_{TH} v > + N(2^3S) \ N_{Cd} < \sigma_p v > - \alpha n_e N(Cd^+) - \frac{D_+ \ N(Cd^+)}{\Lambda^2 p} \qquad (7.9)$$

Equation (7.9) was solved numerically in conjunction with equations (7.2) and (7.4), the rate equations governing the helium ion and 2^3S metastable densities. In order to simplify the evaluation of this system of coupled differential equations, the metastable density decay was simplified further to

$$\frac{dN(2^3S)}{dt} = - N(2^3S) \ N_{Cd} < \sigma_p v > \qquad (7.10)$$

for this calculation only.

Using the recombination rate coefficient given in section 6.5.1 and an assumed electron temperature of 1000 K, this system of coupled equations was solved for initial electron, ion and metastable densities

corresponding to the discharge conditions given in Figure 7.1c; however, the solutions did not agree with the experimental results.

As the Penning ionization and thermal energy charge transfer rates have been extensively studied whereas no detailed study has been undertaken of the cadmium ion-electron recombination process, it was decided to adjust the recombination coefficient (α) so that theory and experiment agreed. The value for the recombination coefficient required was

$$\alpha = 2.7 \times 10^{-6} \text{ cm}^3 \text{ sec}^{-1}$$

which is substantially larger than the value expected from Hinnov and Hirschberg (1962).

Using this value for the recombination coefficient the results of the calculation suggest that, in the early afterglow, the ion density does increase above the steady state value but the increase is such that the condition (7.8) is valid during the first 10 μsec where electronic processes are important. Condition (7.8) does not apply late in the afterglow where the cadmium ions are the dominant ion species but, at these times, electron collision processes will not be significant.

Thus, the electron density decay can be approximated by

$$n_e \simeq N(He^+) \qquad (7.11)$$

throughout the afterglow.

7.2.5 Decay of the Electron Temperature

In the afterglow the electron temperature may relax as a result of electron-neutral and electron-ion collisions and wall losses. On the

other hand, because of the relatively large densities of excited species in the discharge, the collision processes

$$He(2^3S) + e \rightarrow He(1^1S_0) + e + 19.8\ eV$$

$$He(2^1S) + e \rightarrow He(^1S_0) + e + 20.6\ eV$$

$$He(2^1S) + e \rightarrow He(2^3S) + e + 0.79\ eV$$

$$He(2^3S) + He(2^3S) \rightarrow He^+ + He + e + 15.0\ eV$$

are all sources of electron heating in the early afterglow and must be considered in the energy balance equations for the electrons. Following Deloche et al. (1976), the rate equation governing the evolution of the electron temperature in the afterglow can be written as

$$\frac{dT_e}{dt} = a \frac{T_g}{p} \nabla (T_e^{\frac{1}{2}} \nabla T_e) - b_1 \frac{p}{T_g} T_e^{\frac{1}{2}} (T_e - T_g) - b_2 N(He^+) T_e^{3/2}$$

$$x (T_e - T_g) \ln \left(b_3 \frac{T_e^{3/2}}{T_g^{\frac{1}{2}}}\right) + c_1 \left(\frac{T_g}{p}\right)^{\frac{1}{2}} \delta_1 \left(\frac{T_e}{T_g}\right)^2 n_e^{\frac{1}{2}} N(2^3S)$$

$$+ \frac{T_g}{p} n_e^{\frac{1}{2}} d_{11} \beta_{11} [N(2^3S)]^2 \qquad (7.12)$$

where the first term represents thermal conductivity, the second and third terms energy loss through electron-neutral and electron-ion collisions and the last two terms the heating due to electron-metastable superelastic collisions and metastable-metastable ionization. Heating due to superelastic collisions between electrons and the singlet metastable species has been neglected because of the small concentration of these atoms coupled with the fact that the primary loss mechanism is singlet to triplet conversion relinquishing only 0.79 eV of energy to the

electron gas. The constants, a, b_1, b_2, b_3, c_1, δ_1, d_{11} and β_{11} have been determined by Deloche and the values are given in Table 7.1.

TABLE 7.1

Constants Used in Evaluating Equation 7.12

PARAMETER	VALUE	UNIT
a	75.61	cgs
b_1	1.22×10^{6}	cgs
b_2	9.89×10^{-4}	cgs
b_3	8.26×10^{3}	cgs
c_1	1.07×10^{-2}	cgs
δ_1	4.2×10^{-9}	cm^3/sec
d_{11}	5.36×10^{-3}	cgs
β_{11}	1.5×10^{-9}	cm^3/sec

An examination of the solution of equation (7.12) suggests that the electron temperature in the early afterglow increases, primarily due to electron-metastable superelastic collisions, with the electron temperature rising from the initial estimate of 1000 K to 2000 K after approximately 10 μsec and thereafter decreasing. A variable electron temperature would normally require continuous recalculation of the superelastic collision and recombination rate coefficients and use more computer time than the quality of the data would justify. However, the superelastic collision rates are relatively insensitive to temperature variations in the range 1000 - 2000 K and although recombination is a strong function of electron temperature it has been deleted from the

simplified description of the afterglow. In these circumstances the electron temperature has been assumed to be constant throughout the afterglow.

7.3 DISCUSSION

7.3.1 Qualitative Description of the Model

A schematic diagram, showing the collision mechanisms represented by the simplified set of rate equations, is given in Figure 7.2.

In the early afterglow the electron density is high ($\sim 10^{13}$ cm^{-3}) and the electron temperature low ($\sim$1000 K). As a result of this, He (2^3S) production occurs via conversion of the 2^1S, 2^1P and 2^3P levels through electron knockdown and radiative decay. As the major steady state loss mechanism is that of ionization and this process can not occur in the afterglow, the initial losses from the 2^3S metastable level (through superelastic collisions and Penning ionization) are less than in the d.c. discharge and thus the metastable density will increase. Some microseconds later the production rate falls, due to the rapid depletion of the 2^1S, 2^1P and 2^3P populations, whereas the losses through electron superelastic collisions and Penning ionization remains virtually unchanged. Thus, following the initial increase in density, there is a period where the metastable loss is controlled by the combination of Penning ionization diffusion and electron knockdown resulting in a faster than linear decay on a semi-logarithmic scale. Late in the afterglow the electron density has decayed to such a small level that loss by superelastic collisions is unimportant and the 2^3S decay is determined solely by Penning ionization and diffusion. In this region the

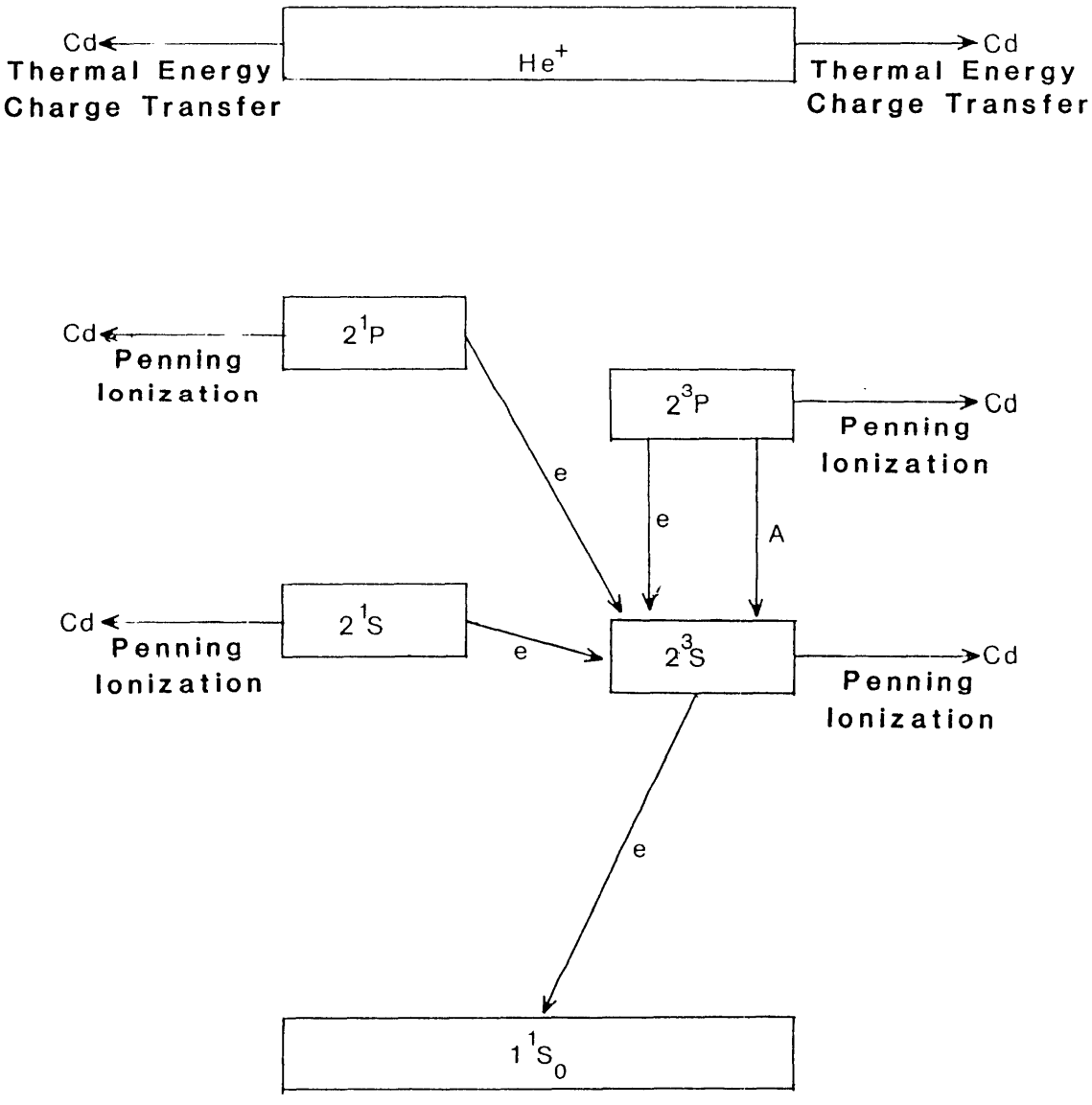

Figure 7.2 A schematic diagram showing the collision mechanisms represented by the simplified set of rate equations developed in section 7.2

metastable density can be expected to decay linearly (on a semi-logarithmic plot).

7.3.2 Dependence on Cadmium Concentration

As discussed in section 4.5.1, increasing the cadmium concentration resulted in a decrease of the relative peak height of the 4416 Å decay. At the same time, all 4416 Å decay curves exhibited an early non-linear decay (on the semi-logarithmic plot) followed, late in the afterglow, by a linear tail.

Increasing the cadmium concentration has two effects on the 2^3S population. Firstly, the Penning collision rate out of the high lying helium levels increases, reducing the number of these atoms converted to the metastable level and hence diminishing the magnitude of the 2^3S density increase. Secondly, the addition of cadmium to the discharge reduces the electron temperature thus increasing the electron knockdown rate.

The reduction in relative peak height is then seen to be due to the fact that Penning collisions deplete the 2^1S, 2^1P and 2^3P levels faster than they are converted to 2^3S. The existence of the non-linear decay region at all oven temperatures is due to the fact that increases in the Penning collision rate are also matched, because of the decreasing electron temperature, by increases in the electron superelastic collision rate. Late in the afterglow the electron collision processes become unimportant and we are left with Penning collisions and diffusion alone determining the decay.

Evidence supporting this decrease in electron temperature and

consequent increase in the superelastic collision rate comes from a re-examination of the 4416 Å decay. Choosing times on the non-linear decay for which the 2^3S production is effectively zero but electron processes are still important, drawing the tangent to the curve allows a calculation of the instantaneous loss rate at that time. This loss rate consists of contributions from both electron de-excitation and Penning ionization; the latter may be subtracted and hence the electron de-excitation rate estimated. If it is further assumed that the electron density has not decayed much from its initial value then the value of the electron temperature at this time can be determined thus providing a crude estimate of T_e for d.c. conditions. Results of these calculations are shown in Table 7.2.

TABLE 7.2

Estimated Electron Knockdown Rates and Derived Electron Temperature as a Function of Oven Temperature

OVEN TEMPERATURE ^oC	ELECTRON KNOCKDOWN RATE $(sec)^{-1}$	ELECTRON TEMPERATURE (K)
225	2×10^4	7000
250	2.4×10^4	6000
275	5×10^4	3000
300	1.3×10^5	1000

The temperature values were calculated by choosing an electron temperature such that the electron knockdown rate, calculated from the semi-empirical cross section data of Fujimoto (1978) and an assumed

Maxwellian velocity distribution for the electrons, fitted the experimental results.

The results are consistent with a reduction in electron temperature with increasing cadmium concentration but the values at low cadmium densities are very much larger than those obtained when LTE is assumed (Chapter 3).

7.3.3 Dependence on Discharge Current

At low oven temperatures, increasing the discharge current resulted in a decrease of the relative peak height of the 4416 Å decay (4.5.2) and a decrease (relative to the steady state intensity) in the point of intersection of the extrapolated linear tail with the T=0 axis. For convenience Figure 7.3 repeats the current dependence of the 2^1S, 2^1P, 2^3S and 2^3P levels given in Chapter 3. As shown in Figure 7.3, the He (2^3S) density increases approximately linearly for currents up to ∿150 mA/anode after which the density saturates and remains constant. The 2^1S, 2^1P and 2^3P levels, on the other hand, remain very nearly constant. At low currents the 2^1S, 2^1P and 2^3P densities are a significant fraction (∿30%) of the 2^3S density and thus conversion of these populations will provide a significant increase in the triplet metastable density. As the current is increased, the 2^3S density increases whereas the 2^1S, 2^1P and 2^3P densities remain constant and thus conversion of the latter will lead to a proportionally smaller increase in the metastable density.

The current dependence of the point of intersection of the extrapolated linear tail with the T=0 axis can be explained in terms of the current dependence of the electron density. With increasing discharge current the electron density increases linearly (Chapter 3) and

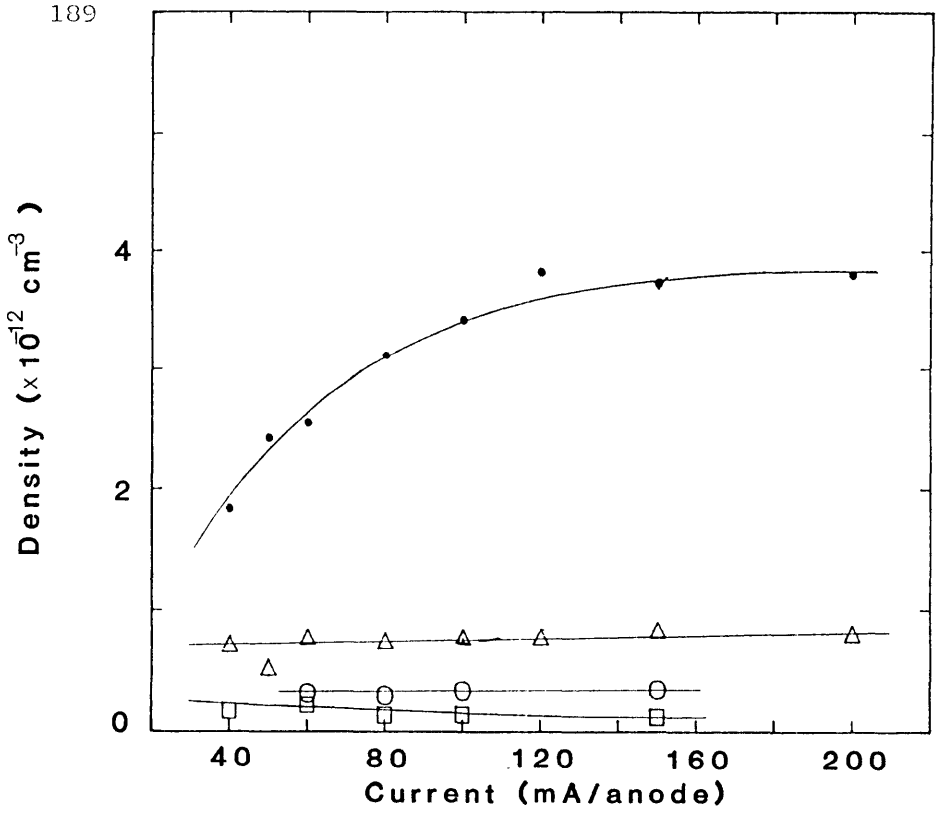

Figure 7.3 Current dependence of the 2^3S (•), 2^1S (Δ), 2^1P (0) and 2^3P (□) densities in a "pure" helium discharge at a gas pressure of 20 Torr

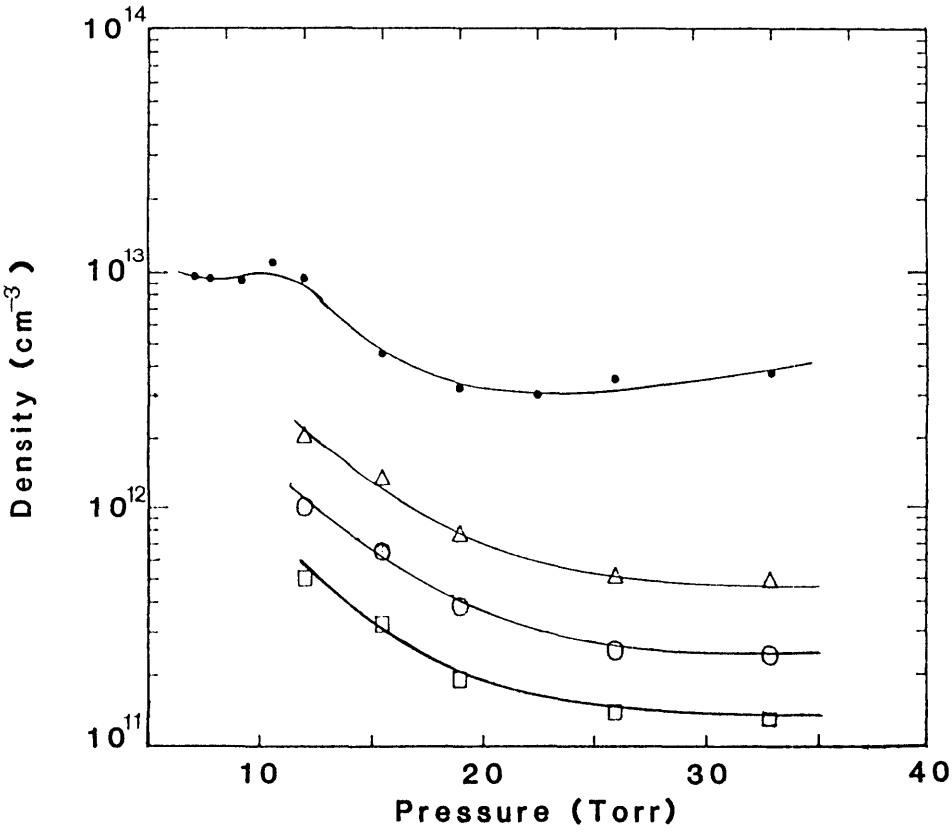

Figure 7.4 Pressure dependence of the 2^3S (•), 2^1S (Δ), 2^1P (0) and 2^3P (□) densities in a "pure" helium discharge at a current of 120 mA/anode

thus the electron de-excitation rate will become more significant. With a large loss through electron knockdown and an almost constant Penning rate the metastable density is reduced to lower values before electron processes become insignificant. This will result in the shift in the point of intersection of the extrapolated linear tail with the T=0 axis.

7.3.4 Dependence on Helium Pressure

With increasing pressure the relative peak height remains very nearly constant and the point of intersection of the linear tail extrapolated to the T=0 axis decreases relative to the steady state value.

Figure 7.4 shows the pressure dependence of the helium 2^3S, 2^3P, 2^1P and 2^1S densities. With increasing pressure the densities of all levels decrease but the relative populations remain nearly constant. Thus, the percentage increase in the population of the 2^3S level (as a result of conversion of the higher levels) will remain constant and so will the relative peak height.

As discussed in section 4.5.3, increasing the helium pressure results in an increase in the electron density and, to some extent a reduction in the electron temperature, leading to an increase in the electron knockdown rate in the early afterglow. With an increase in the knockdown rate and a constant Penning collision rate, the metastable density is reduced more rapidly in the early afterglow. This will result in the observation that the point of intersection of the extrapolated linear tail with the T=0 axis decreases relative to the steady state value.

7.4 ELECTRON DE-EXCITATION OF THE $5s^2\ ^2D_{5/2}$ LEVEL OF Cd II

In the preceding discussion it has been assumed that the dominant loss mechanism is that of radiative decay and no consideration has been given to the role of slow electron collisions in depopulating the $5s^2\ ^2D_{5/2}$ level of Cd II. Mori, Murayama, Goto and Hattori (1978) and Hane et al. (1982) have both concluded that electron de-excitation must be included in the loss processes of the $5s^2\ ^2D_{5/2}$ level. This is further supported by Browne (1972), who measured a non-radiative decay rate for the $5s^2\ ^2D_{5/2}$ level of $\sim 10^6$ sec^{-1}.

In view of the fact that no accurate data are available for the collision cross section, electronic de-excitation has not been included explicitly in the discussion of the He-Cd afterglow. However, inclusion of electron knockdown of the $5s^2\ ^2D_{5/2}$ level would only result in an enhancement of the early non-linear decay and would not invalidate the preceding discussion.

7.5 SOLUTION OF THE SIMPLIFIED COUPLED DIFFERENTIAL RATE EQUATIONS

The system of coupled differential equations describing the afterglow, equations 7.2, 7.4, 7.6, and 7.11, have been solved using a computer based numerical technique. Estimates of the rate coefficients and initial population densities required for the analysis are summarized in Table 7.3.

Output, showing the calculated 2^3S metastable density as a function of time, is given in Figure 7.5. Also shown is the 4416 Å spontaneous

TABLE 7.3

Densities and Rate Coefficients Used in Evaluation of the Coupled Rate Equations

OVEN TEMPERATURE 250^0 C

Parameter	60 mA/anode	120 mA/anode	180 mA/anode	Comments
2^3S (cm^{-3})	1.8×10^{12}	3.8×10^{12}	3.4×10^{12}	Estimated from experimental results of Chapter 3
2^1S (cm^{-3})	5.0×10^{11}	5.0×10^{11}	5.0×10^{11}	
2^1P (cm^{-3})	2.5×10^{11}	2.5×10^{11}	2.5×10^{11}	
2^3P (cm^{-3})	2.0×10^{11}	2.0×10^{11}	2.0×10^{11}	
N_{Cd} (cm^{-3})	1×10^{14}	1×10^{14}	1×10^{14}	From SVP equations
$n_e = N_{He^+}$ (cm^{-3})	1×10^{13}	2×10^{13}	3×10^{13}	Estimated from experimental work of Gill and Webb (1978) and Belal and Dunn (1978)
T_e (K)	1000	1000	1000	Estimated from experiment
T_g (K)	650	950	1050	From gas temperature measurement of Appendix A2
$A_{2^3P-2^3S}$ (s^{-1})	0.094×10^{8}	0.094×10^{8}	0.094×10^{8}	Wiese, Smith and Glennon (1966)
$R_{de\text{-}ex}$ (cm^3s^{-1})	1.2×10^{-9}	1.2×10^{-9}	1.2×10^{-9}	Estimate from section 7.3.2
$R_{conv}^{2^1S}$ (cm^3s^{-1})	6×10^{-7}	6×10^{-7}	6×10^{-7}	Cross section data of Fujimoto (1978) and an assumed Maxwellian velocity distribution
$R_{conv}^{2^1P}$ (cm^3s^{-1})	1×10^{-8}	1×10^{-8}	1×10^{-8}	
$R_{conv}^{2^3P}$ (cm^3s^{-1})	4×10^{-7}	4×10^{-7}	4×10^{-7}	
σ_p (cm^2)	4.5×10^{-15}	4.5×10^{-15}	4.5×10^{-15}	Schearer and Padovani (1970)
σ_{TH} (cm^2)	3.7×10^{-15}	3.7×10^{-15}	3.7×10^{-15}	Collins *et al.* (1971)

TABLE 7.3 (continued)

OVEN TEMPERATURE 275^{0}C

Parameter	120 mA/anode	Comments
2^3S (cm^{-3})	1.70×10^{12}	Estimated from experimental results of Chapter 3
2^1S (cm^{-3})	3.5×10^{11}	
2^1P (cm^{-3})	8×10^{10}	
2^3P (cm^{-3})	1×10^{11}	
N_{Cd} (cm^{-3})	3×10^{14}	From SVP equations
R_{de-ex} ($cm^3 sec^{-1}$)	3×10^{-9}	Estimate from section 7.3.2

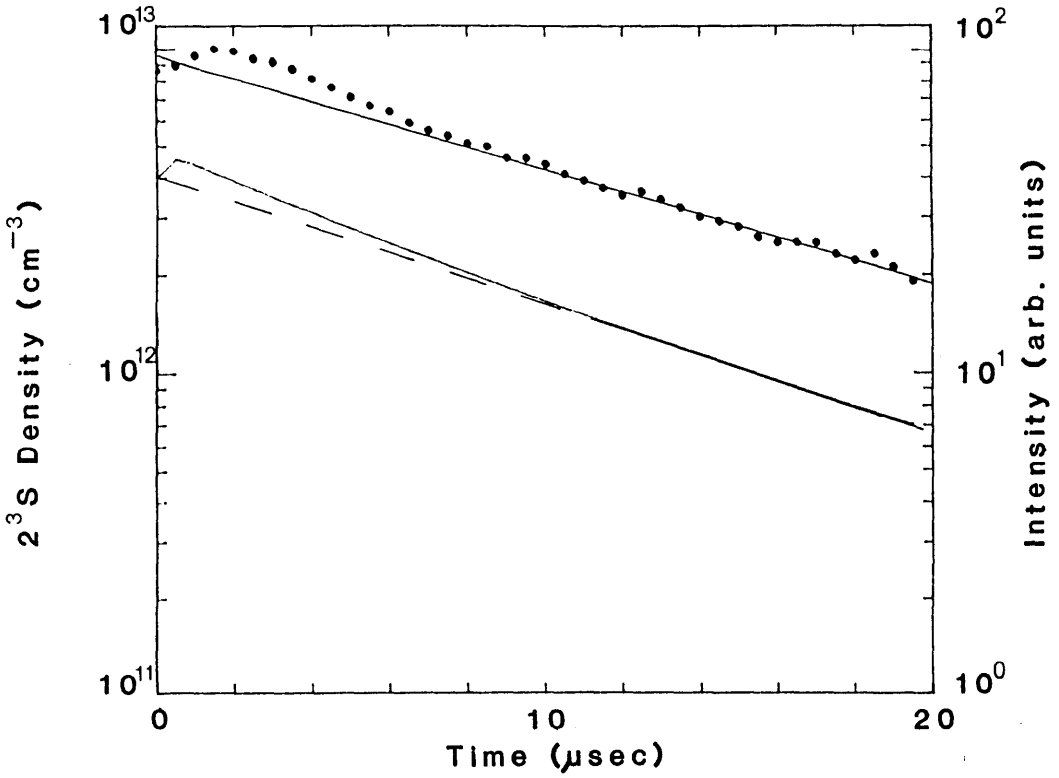

Figure 7.5 Comparison of the 2^3S metastable density decay (——) calculated from the coupled rate equations with the corresponding decay of the 4416 Å transition (•). Conditions: 250°C oven temperature, 120 mA/anode, and a pressure of 20 Torr helium

emission for the discharge conditions corresponding to the parameters used in the calculation. Clearly, the rate equations predict that the metastable density follows closely that of the 4416 Å spontaneous emission. The program does not accurately predict the time to peak intensity, most probably due to uncertainties in the data used, but it does predict time to onset of the linear decay region which are in reasonable agreement with the experimental observations.

To provide a further check on the accuracy of the simplified model the output from the coupled rate equations was investigated as the initial conditions were varied in a manner consistent with a change in the discharge current. The currents investigated were with 60 mA/anode, 120 mA/anode and 180 mA/anode and the corresponding outputs are shown in Figures 7.6a - 7.6c. With increasing current the relative peak height of the metastable density is decreased and the point of intersection of the linear tail with the T=0 axis is shifted downwards with respect to the steady state density. This is in complete agreement with the experimental results.

Figures 7.7a - 7.7b show the output of the coupled differential rate equations corresponding to two different cadmium concentrations. Again, the percentage metastable density increase is reduced while the shape of the metastable decay remains invariant.

Thus the system of coupled differential equations developed in section 7.2 does, for reasonable estimates of the collision rates and initial densities, predict the experimentally observed trends of the 4416 Å spontaneous emission.

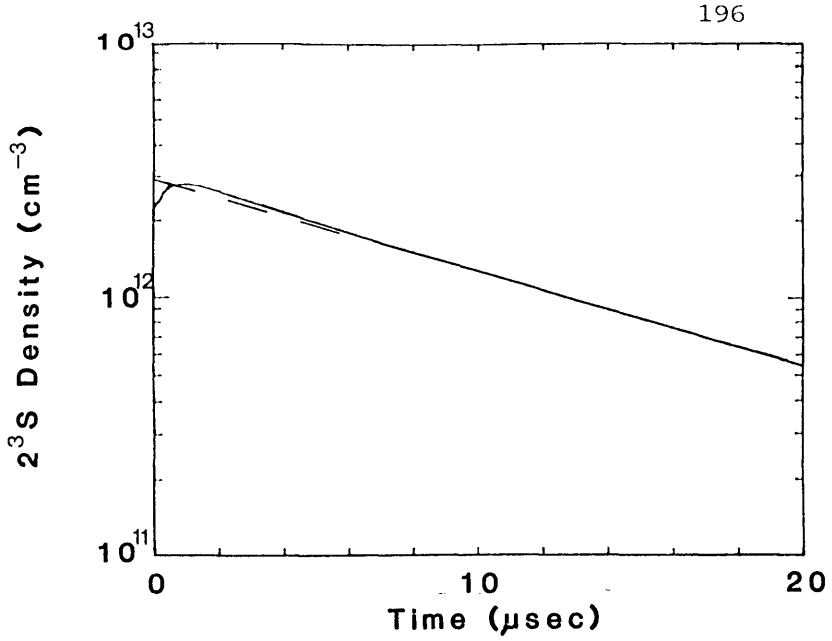

Figure 7.6a
Calculated 2^3S metastable density at a current of 60 mA/anode, 250°C oven temperature and a pressure of 20 Torr

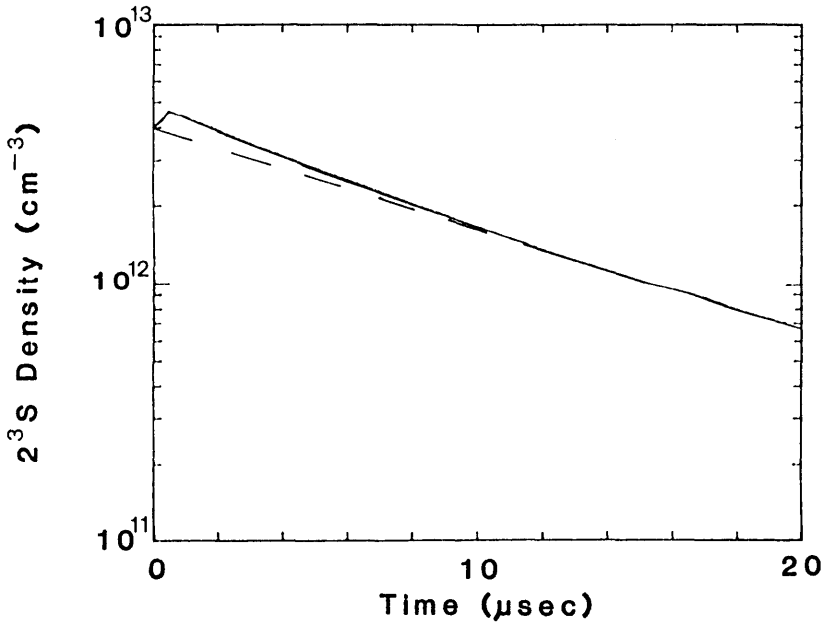

Figure 7.6b
Calculated 2^3S metastable density at a current of 120 mA/anode, 250°C oven temperature, and a pressure of 20 Torr

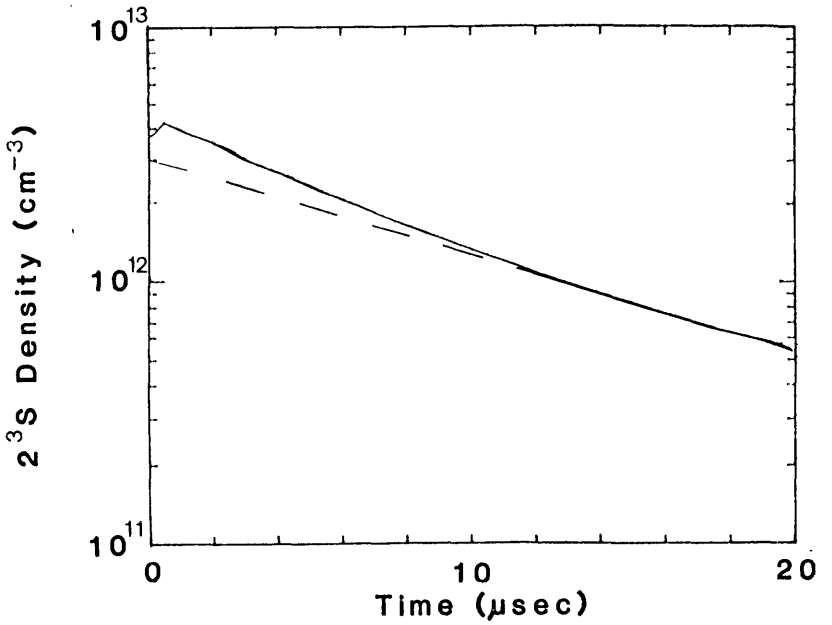

Figure 7.6c
Calculated 2^3S metastable density at a current of 180 mA/anode, 250°C oven temperature and a pressure of 20 Torr

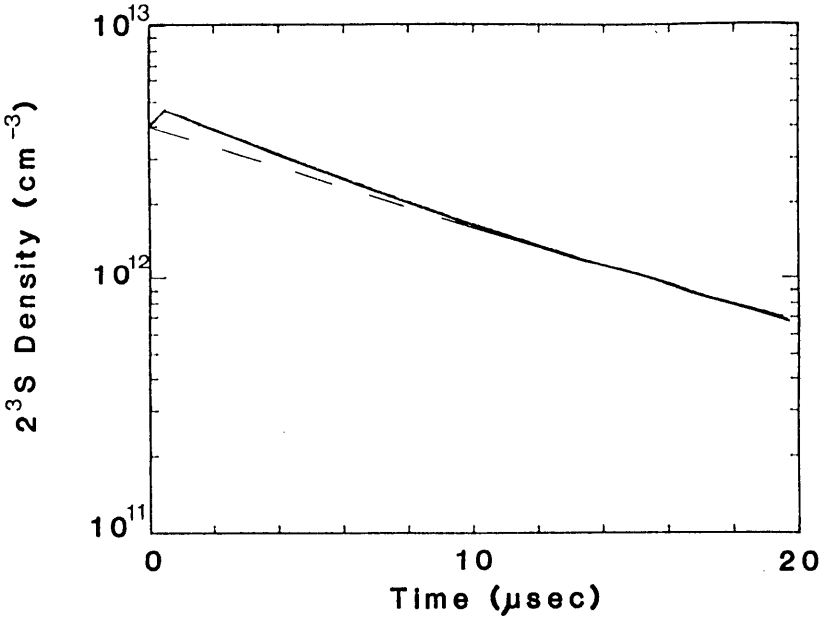

Figure 7.7a
Calculated 2^3S metastable density at an oven temperature of 250°C, 120 mA/anode discharge current and a pressure of 20 Torr

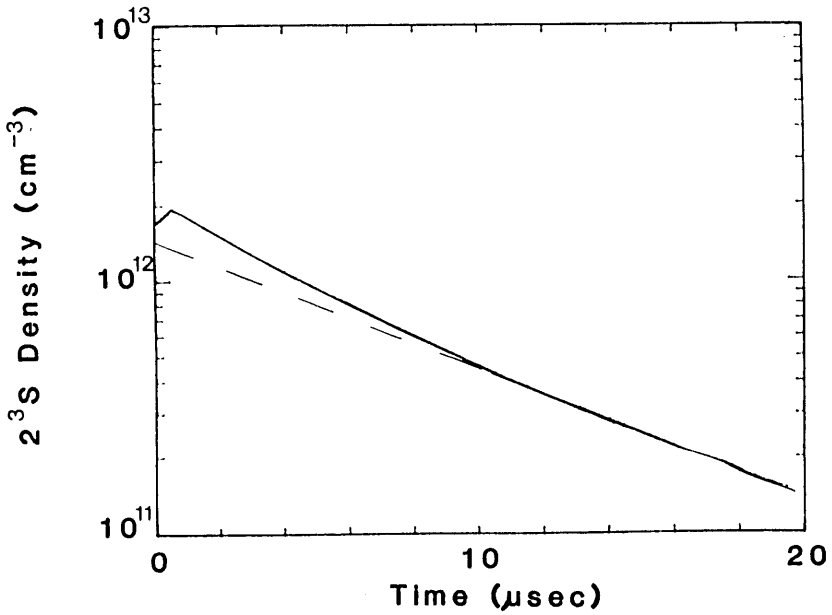

Figure 7.7b
Calculated 2^3S metastable density at an oven temperature of 275°C, 120 mA/anode discharge current and a pressure of 20 Torr

7.6 DIRECT EXPERIMENTAL EVIDENCE FOR AN INCREASE IN THE 2^3S POPULATION IN THE EARLY AFTERGLOW

These calculations predict that the 2^3S density increases in the early afterglow. The only practical way to check this is via direct measurement of the 2^3S population and, as mentioned in Chapter 5, the RC limitations placed on the detection system made measurement of the 2^3S density in the early afterglow extremely difficult. To overcome the RC limitations the 22 kΩ photomultiplier output resistance was reduced to 3.3 kΩ. In doing this the response time of the detection system is reduced to ∿1 μsec but the available signal is also reduced sevenfold. To overcome the reduction in signal strength the intensity regrowth signal was accumulated over a period of 40 minutes (at 1 Hz repetition rate) and for experimental conditions where both the absorption and 3889 Å intensity are maximized (at low cadmium concentrations).

The result of the experiment is shown in Figure 7.8. Careful examination of the data shows that in the early afterglow the absorption appears to increase before decaying and there is thus some evidence that the 2^3S population does indeed increase in this region.

7.7 SUMMARY

To explain the decay of the 4416 Å spontaneous emission it was proposed that Penning collisions between He (2^3S) metastable atoms and cadmium neutral atoms excite the upper level, the $5s^2\ ^2D_{5/2}$ level, of this transition and that the observed intensity variations of this decay mirror those changes in the 2^3S population in the afterglow. In this chapter the rate equations for the important excited and ionic ground

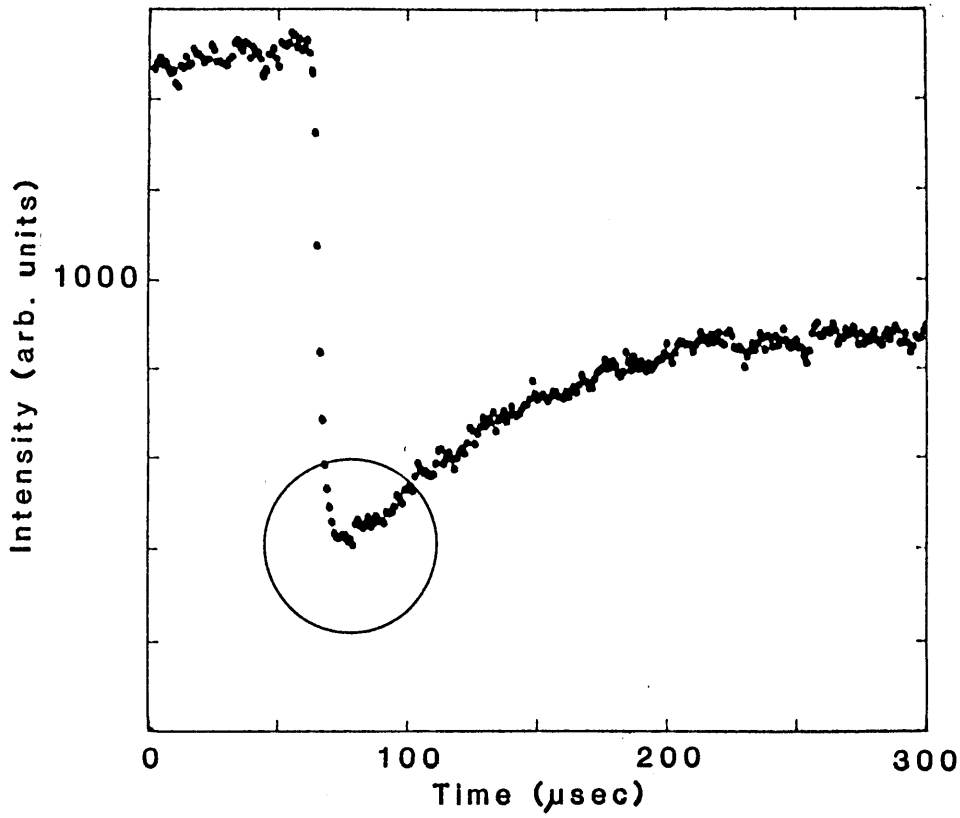

Figure 7.8 *3889 Å intensity regrowth curve at an oven temperature of 225°C, 120 mA/anode discharge current and a pressure of 20 Torr helium. Circled area contains some evidence of an increase in the absorption before the subsequent decay. Each data point represents a time interval of 1 μsec*

states of helium and the electron temperature and density were developed. Incorporated in these rate equations were processes, such as electron de-excitation of the 2^3S level to the helium ground state and conversion of the higher lying levels to the 2^3S, which were shown to occur at a significant rate in the afterglow of the hollow cathode discharge.

The model was used to explain qualitatively the observed decay of the 4416 Å spontaneous emission. The intensity increase was seen to be a result of the fact that the 2^3S metastable production, via conversion of the higher lying levels by radiative decay and collisions of the second kind, is maintained in the early afterglow whereas the metastable losses are greatly reduced as electron impact ionization is no longer possible. As the densities of the higher lying levels were shown to be a significant (30-40%) fraction of the 2^3S, the density of the 2^3S level increases above that of the steady state discharge. Further, because the rate coefficient for electronic de-excitation of the 2^3S level is of the same magnitude as that for Penning collisions, losses via this mechanism are also significant in the early afterglow when the electron density is large. Thus, following the initial period where metastable production is maintained (1-2 μsec) the decay of the 2^3S level is determined by electronic de-excitation, Penning collisions and diffusion and is therefore more rapid than if the latter two processes alone operated. Late in the afterglow the He (2^3S) decay, and hence 4416 Å decay, is determined by Penning collisions and diffusion as electronic processes cease due to the rapid decay of the electron density.

The proposed model also qualitatively accounted for the current, pressure and cadmium concentration dependence of the 4416 Å decay explaining the parametric variation of both the relative peak height and the point of intersection of the extrapolated exponential tail with the

afterglow initiation axis.

Finally, using the available data for densities of the excited states of helium, the electron density and collision cross sections along with estimates for the electron temperature and electron energy distribution function, the set of coupled differential rate equations developed for the afterglow was solved numerically. In view of the incompleteness of the data and the uncertainty associated with the functional form of both the electron velocity distribution and collision cross section data, agreement between the experimental results and predicted decay of the 2^3S density was remarkable. Indeed, from this study one could only conclude that the He (2^3S) density does indeed have a temporal evolution identical to that of the 4416 Å decay in the afterglow of the He-Cd^+ hollow cathode discharge. Further, the current, pressure and oven temperature dependence of the decay were also replicated.

Thus, while difficulties forced us to model the afterglow region to explain the experimental observations, the results of this approach were fruitful. The Penning collision mechanism alone excites the $5s^2\ ^2D_{5/2}$ level of Cd II in the afterglow of a He-Cd^+ hollow cathode discharge and this result, along with the experimental data of Chapter 4, reinforces the earlier conclusion that the Penning collision mechanism alone excites this level in the d.c. discharge.

CHAPTER 8

CONCLUSION

8.1 SUMMARY

In this thesis spectroscopic studies of a hollow cathode He-Cd^+ discharge have been presented and discussed. Investigations were carried out in both the d.c. discharge and corresponding afterglow, the major aim being to ascertain the importance of the Penning collision mechanism represented by

$$He(2^3S) + Cd(1^1S_0) \longrightarrow He(1^1S_0) + Cd(5s^2\,^2D_{5/2}) + e$$

in populating the $5s^2\,^2D_{5/2}$ level of the cadmium ion, the upper level of the 4416 Å laser transition. Determining whether the Penning collision mechanism, or some second collision process such as electronic excitation, is responsible for populating this level is important as this will help resolve whether the laser power saturation observed by a number of researchers (Grace and McIntosh, 1979; Takasu et al., 1982) is a fundamental discharge limited phenomenon or whether it could be eliminated with suitable design considerations.

In this chapter, the results obtained will be briefly reviewed and the implications of the results to the stated aims of the study assessed. In view of the nature of these studies, the summary will be divided into two subsections: the steady state discharge and the afterglow. This is then followed by some concluding remarks summarizing the implications of the present study and suggestions for future research.

8.2 STEADY STATE DISCHARGE

The investigation of the steady state discharge was limited to measurement of the parametric variation with discharge current, helium pressure and cadmium concentration of relevant excited state helium densities, the cadmium ion ground state density and the 4416 Å spontaneous emission. Population density measurements of the helium 2^3S and 2^1S metastable levels, the 2^1P and 2^3P levels of neutral helium (being the next most highly excited levels of helium) and the cadmium ion ground state density were made using the absorption spectroscopy technique of fractional absorption described and developed in Chapter 2. Results of this investigation, of the helium and helium-cadmium discharges, were presented in Chapter 3.

8.2.1 Helium Discharge

In the helium discharge, for a constant pressure, the He (2^3S) density was observed to increase almost linearly up to a current of 100 mA/anode after which density saturation occurred. This saturation, with increasing current, was explained using a simple model taking into account metastable production via electronic excitation from the ground and higher lying helium levels and losses by diffusion, ionization through electronic collisions and electronic de-excitation to the ground state. On the other hand, the densities of the helium 2^1S, 2^1P and 2^3P levels were very nearly independent of discharge current having values of approximately an order of magnitude smaller than the 2^3S level. This result was particularly significant as one would normally expect the

difference between the 2^3S and 2^1S densities to be only one third and the fact that it was much less supports the view that singlet to triplet metastable conversion provides a major loss mechanism for the He (2^1S) level. This conversion relies on the existence of a significant number of slow thermal electrons in the hollow cathode discharge; such electrons are particularly efficient in de-exciting higher lying levels and the observation of their effects in the d.c. discharge was confirmed by later observations of them performing precisely this role in the early afterglow.

At a constant current, the densities of the 2^3S, 2^1S, 2^1P and 2^3P levels were found to decrease for pressures greater than 8 Torr but the relative population densities remained very nearly constant. This decrease was attributed to an increase in the collisional de-excitation and ionization rates due to a combination of a decrease in the mean energy of the electrons together with an increase in the electron density.

8.2.2 Helium-Cadmium Discharge

With the addition of cadmium to the discharge volume, the densities of all the helium levels investigated fell, decreasing by approximately two orders of magnitude over the oven temperature (cadmium concentration) range covered. This decrease was interpreted in terms of an increase in the loss mechanisms due to Penning ionization (the rate of which is approximately proportional to the cadmium concentration), and de-excitation and ionization to the neutral and ion ground states respectively. These last two processes are enhanced by the introduction of a low ionization potential material such as cadmium to the discharge because this shifts the thermal energy peak of the electron energy

distribution function to lower energies, thus increasing the collision rates for these electronic processes.

For a constant cadmium concentration, the 2^1S, 2^1P, 2^3S and 2^3P levels exhibited current and pressure dependences similar to those observed in helium except that the curves had been shifted to lower values. The only significant difference was that the saturation current for the He (2^3S) metastable density was shifted to a higher value, a result which was readily explained by including the Penning collision mechanism in the rate equation governing the metastable density.

In these density measurements, the effects of gas temperature variations with current, pressure and cadmium concentration were taken into account. Variations in the value of T_g proved to have a significant effect on the excited state density calculated from the absorption data, because equation 2.6 (relating the experimentally determined absorption coefficient to the excited state densities) directly involves the Doppler width which is proportional to $(T_g)^{\frac{1}{2}}$. The gas temperature was determined from the structure of the rotational spectrum of a small amount of impurity N_2 present within the discharge and was found to increase linearly with current, doubling over the current range investigated, and thus resulting in approximately a 50% variation in the Doppler width. No significant pressure dependence of T_g was observed.

These density measurements were made in order that the Penning collision rate could be calculated and compared with the corresponding parametric variations of the 4416 Å spontaneous emission, thus assessing the importance of Penning collisions in populating the upper level of this transition.

Past investigators have attempted this comparison by assuming that

the variations in the Penning rate exactly follow those of the helium 2^3S density. As a function of pressure, at a constant current and cadmium concentration, I_{4416} exhibited a similar dependence to that of He (2^3S) initially suggesting that the Penning collision mechanism dominates production of the $5s^2\ ^2D_{5/2}$ level. However, closer examination of the ratio I_{4416}/He (2^3S) showed a factor of 2-3 variation over the pressure range investigated which is indicative that a second collision process, such as electronic excitation, could be predominant at the higher pressures. For a constant helium pressure and cadmium concentration, the current dependence of the He (2^3S) density rose approximately linearly up to a current of 140 mA/anode then saturated whereas the corresponding curve of I_{4416} rose nearly linearly. These results have previously been used as clear evidence to support the view that electronic excitation of the $5s^2\ ^2D_{5/2}$ level is significant. At a constant pressure and current, the curves of I_{4416} and the product N_{cd}.He (2^3S) exhibited similar characteristics with any slight discrepancies being associated with the values of He (2^3S) and N_{cd} used in the calculation.

These conclusions are based on the untested assumption that the Penning rate is independent of discharge parameters. In fact, the Penning rate depends not only on the cross section but also on the mutual velocity of the collision partners and thus on the gas temperature. In the present experiments, gas temperature was found to be a function of discharge parameters, especially current, and the assumption used by previous investigators is inadequate.

Provided that the collision cross section is independent of gas temperature then the Penning collision rate is not constant but rather is proportional to $(T_g)^{\frac{1}{2}}$. This result does not significantly affect the previous conclusions drawn from comparisons of I_{4416} with the Penning

collision rate for variations of pressure and cadmium concentration, because T_g is only weakly dependent on these parameters. However, because T_g depended linearly on current, its inclusion in the calculation of the Penning collision rate significantly alters the conclusions drawn from a comparison of the graphs of I_{4416} and the Penning collision rates as the collision rate is now represented by the product He $(2^3S) \times T_g^{\frac{1}{2}}$ rather than He (2^3S). Inclusion of the gas temperature effects on the Penning collision rate largely removed the discrepancies between these two curves making the evidence supporting the role of electron excitation processes less convincing. There is still, however, approximately a 40-50% variation of the ratio $I_{4416}/[\text{He } (2^3S) \times T_g^{\frac{1}{2}}]$ and thus, while inclusion of the gas temperature removed the "conclusive" evidence supporting the view of the role of a second collision mechanism it has by no means provided conclusive evidence supporting the hypothesis that Penning collisions alone are responsible for excitation of the $5s^2\ ^2D_{5/2}$ level.

8.2.3 Discussion

The experimental observations of the present study of the steady state discharge are in agreement with those of Grace and McIntosh (1979), Takasu et al. (1982) and Gill and Webb (1978). For those based on a comparison of the current dependence of the 2^3S density and 4416 Å spontaneous emission, these authors had concluded that electron excitation is not insignificant. We now believe that this conclusion is, in fact, not fully substantiated because these authors had not taken into account either or both of the dependence of the Doppler width or Penning collision rate on gas temperature.

This conclusion does, however, conflict with the work of Mori, Goto and Hattori (1978) and Mori, Murayama, Goto and Hattori (1978) who deduced that, in a positive column discharge, a significant fraction of the $5s^2\ ^2D_{5/2}$ population was due to electron impact excitation from the cadmium ion ground state. In view of the fact that the helium metastable and cadmium neutral densities are of similar magnitudes in the hollow cathode discharge used in this present study and the positive column device used by Mori and his co-workers (1977, 1978a, 1978b) but the electron density is nearly two orders of magnitude smaller in the latter than the former, the conclusion reached by Mori and his colleagues is surprising. It should be noted that Mori et al. measured the He (2^3S) density to be independent of discharge current, a result which differs significantly from the earlier studies by Browne and Dunn (1973) and Mizeraczyk (1975), also in a positive column discharge. Although it could be argued that the electronic excitation rate in the positive column discharge will be large because the peak in the electron energy distribution occurs close to where the collision cross section is a maximum, the distribution function of the positive column has very few high energy electrons whereas that of the hollow cathode has an appreciable high energy tail. Hence the excitation rates in these two discharge types may not be very different. If this is true, the fact that the Penning collision and electron excitation rate coefficients are similar whereas the electron density is two orders of magnitude lower in the positive column make it difficult to see how electronic collisions can play an important role in these discharge types.

Independent of what occurs in a positive column discharge, further support for the view that the stepwise electron excitation mechanism,

proposed by Mori et al. (1978a, 1978b), is not a significant process in the hollow cathode He-Cd^+ laser comes from a measurement of the cadmium ion ground state density. Results of the experiment, reported in Chapter 3, show that the ion density is low ($\sim 10^{11}$ atoms cm^{-3}). Even though the cross section for electron excitation to excited ion states is high (Hane et al. 1983a, 1983b) the low ion and electron densities will result in only a small contribution from this process.

Finally, when argon was used in place of helium as the buffer gas, little or no spontaneous emission was visible from transitions of the cadmium ion. As the argon metastables have insufficient energy to Penning ionize the $5s^2\ ^2D_{5/2}$ level of Cd II the result is not inconsistent with the view that Penning ionization is the dominant excitation mechanism of this level.

8.3 AFTERGLOW

The results of the study of the steady state discharge were not conclusive in determining whether the excitation of the $5s^2\ ^2D_{5/2}$ level was solely due to Penning ionization or whether electronic excitation also needed to be taken into account. In order to provide further confirmation of the possible excitation pathways a study of the He-Cd^+ hollow afterglow was made.

In these studies fast digitizing and signal averaging techniques were used to record the decay of the 4416 Å endlight intensity and also the intensity regrowth at 3889 Å and 5016 Å in time resolved absorption studies used to determine the He (2^3S, 2^1S) density decay. Experiments were also developed to investigate the role of such processes as recombination, electronic collisional de-excitation and radiative decay

in the afterglow. Finally, computer modelling of the afterglow was carried out in order to assess the accuracy of a proposed model in explaining the experimental results.

8.3.1 4416 Å Decay

In Chapter 4 the results of a study of the 4416 Å spontaneous emission decay, including the dependence upon the discharge current, cadmium concentration and helium pressure, were presented and discussed. If the Penning collision mechanism is solely responsible for populating the $5s^2\ ^2D_{5/2}$ level then the decay of the 4416 Å spontaneous emission should follow that of the He (2^3S) metastable density which, on the basis of a simple model for the afterglow, was expected to decay exponentially.

In all cases, however, the 4416 Å decay was more complex than anticipated, exhibiting an initial intensity increase immediately following the creation of the afterglow followed by a period of rapid decay, finally giving way to an exponential tail in the later afterglow. While the overall shape of the decay was found to be independent of variations in the discharge parameters, though the intensity increase was most pronounced for low cadmium concentrations subtle, but systematic, variations were observed.

For increases in the cadmium concentration the relative peak height (defined as the peak height/d.c intensity) and the time constant of the late afterglow exponential decay were both observed to decrease. The existence of an exponential decay in the late afterglow and the observation that the time constant decreases with increasing cadmium concentration were both consistent with the proposed simple Penning

collision model of the afterglow. On the other hand, this simple model was apparently not adequate to explain the observed variations in the early afterglow.

With increasing current, the relative peak height was found to decrease. At the same time, the point of intersection of the extrapolated exponential tail with the time zero axis (the afterglow initiation point) also decreased. The former result suggested that the intensity increase is not due directly to electron collisions while the converse is true for the latter. Although some variation in the time constant of the exponential tail may have been expected because of an increase in the gas temperature, none was observed perhaps because of the weak intensities at these times in the afterglow.

Variation in the helium pressure, at constant current and cadmium concentration, resulted in a small but reproducible increase in the time constant of the exponential decay. This was attributed to the pressure dependence of the diffusive losses and from the experimental data values for the diffusion coefficient of the He (2^3S) metastable species of

$$D_m = 740 \pm 200 \text{ cm}^2 \text{ Torr}^{-1} \text{ sec}^{-1}$$

and

$$D_m = 1185 \pm 400 \text{ cm}^2 \text{ Torr}^{-1} \text{ sec}^{-1}$$

were derived. These results were in reasonable agreement with those published by Schearer and Padovani (1970). Also, for pressures < 35 Torr, the point of intersection of the extrapolated exponential tail with the time zero axis decreased relative to the steady state intensity after which the trend reversed. As the electron density is expected to increase with pressure up to approximately 35 Torr and thereafter

decrease this result also suggested that electron collisions were again involved in the early afterglow decay mechanisms. The relative peak height, which showed a strong current dependence, remained essentially constant only falling slightly at the higher pressures.

8.3.2 2^3S Decay

The nature of the 4416 Å decay implied that Penning ionization is dominant in the late afterglow whereas in the more complex early afterglow region electronic processes appear to play a significant role. Direct confirmation of the role of the He (2^3S) metastable species in populating the $5s^2\ ^2D_{5/2}$ level in the late afterglow came from a measurement of the 2^3S density using the Ladenburg-Reiche line absorption method. The experimental theory and procedure and the results of this investigation, plus the investigation of the He (2^1S) decay, were presented in Chapter 5.

The He (2^3S) metastable density decay was measured for variations in the cadmium concentration at a constant current and helium pressure. In the afterglow the He (2^3S) density decayed exponentially with a time constant which decreased with increasing cadmium concentration, a result which was consistent with the simple model proposed for the afterglow. Unfortunately, the signals were too weak to show the pressure dependence associated with diffusion. No precise information could be obtained on the nature of the He (2^3S) decay in the early afterglow because the RC response time of the detection system was convoluted with the fast signal response making accurate data analysis at these times impossible.

The measured He (2^3S) decay time constant was compared with that calculated from the proposed model and the available data for the Penning

collision cross section, diffusion coefficients and cadmium concentration. Although there was good agreement at low cadmium concentrations there was not a close correlation between experiment and theory at high cadmium concentrations, a fact which was attributed to the problems in calculating the cadmium ground state density. On the other hand, the time constant for the 4416 Å late afterglow decay was in good agreement with the corresponding decay rate for the He (2^3S) species providing conclusive evidence that the Penning collision mechanism is dominant in populating the $5s^2\ ^2D_{5/2}$ level at these times.

8.3.3 2^1S Decay

The decay in 2^1S metastable density was determined from measurements of the intensity regrowth at 5016 Å. Comparison of the 2^1S decay with the corresponding 2^3S decay showed that the former is destroyed more efficiently in the afterglow. Further, the decay rate increased slightly with cadmium concentration and was clearly non-exponential. On the basis of available cross section data this result was attributed to the process of singlet to triplet conversion dominating the 2^1S loss at low cadmium concentrations and a combination of this plus Penning collisions at higher oven temperatures. As the reverse process was not expected to be energetically possible in the afterglow, this result suggested that a large proportion of the 2^1S population is converted to the 2^3S level in the first few μsec of the afterglow.

8.3.4 Investigation of the Early Afterglow

The results obtained from the study of the decays of the 4416 Å spontaneous emission and the He (2^3S, 2^1S) metastable density highlighted a number of aspects of the afterglow. In the late afterglow the He (2^3S) decay is determined by Penning collisions and diffusion and the excitation of the $5s^2\ ^2D_{5/2}$ level was shown to be solely due to Penning ionization. The rapid decay of the 2^1S density via conversion to the 2^3S level provided a possible mechanism by which the 2^3S density may increase appreciably in the early afterglow. No such increase was, however, detected because of the limited RC response of the detection system. On the other hand, results of current and pressure dependence of the 4416 Å decay suggested that electronic processes play an important role in the early afterglow.

To explain the formation of the intensity increase and subsequent rapid decay in the early afterglow a number of mechanisms were proposed and investigated experimentally and theoretically. The proposed mechanisms and the means used to investigate them were:

1. The existence of a non-uniform Cd II distribution across the hollow cathode discharge having an axial depression. In Chapter 6 radial profile studies of relevant emission lines of Cd II were investigated and showed that, for normal operating conditions, the excited ion densities have an axial maximum decreasing monotonically to the walls. In light of this investigation it was apparent that the existence of non-uniform profiles of Cd^+ could not provide an explanation for the 4416 Å intensity variation in the afterglow.
2. Excitation of the $5s^2\ ^2D_{5/2}$ level as a result of

electron collisional redistribution amongst the higher lying Cd II levels. On the evidence of the inverse current dependence of the relative peak height it was argued that direct excitation of the $5s^2\ ^2D_{5/2}$ level by electronic redistribution of the higher lying Cd^+ levels was also unlikely.

3. Recombination of Cd^{++} and subsequent decay to the $5s^2\ ^2D_{5/2}$ level. Again, in view of the inverse current dependence of the relative peak height it was argued that this mechanism was also unlikely,

and

4. Penning collisions dominate the production of the $5s^2\ ^2D_{5/2}$ level of Cd II and the 4416 Å intensity simply follows the evolution of the He (2^3S) density in the afterglow. A number of possible mechanisms for the production and loss of this level were considered including recombination of He^+, slow electron collisions plus radiative decay of the higher lying He levels and de-excitation of the He (2^3S) metastable to the ground state by collisions of the second kind.

The mechanisms of recombination, slow electron collisions and radiative decay from higher lying He levels and collisional de-excitation of the 2^3S level, all resulting in metastable production and loss in the afterglow, were considered in Chapter 6. Electronic processes, in particular collisions of the second kind, were thought to play an important role in the early afterglow as the initial electron density is high ($\sim 10^{13}$ electrons/cm^3) and the electron temperature low, a result

which is supported by the observation of the rapid 2^1S decay.

To investigate He (2^3S) production via recombination, the decay of transitions in the helium n^3D-2^3P (n>3) series were investigated in both the helium and He-Cd discharges. In helium, all transitions exhibited a temporal response typical of recombination, with an initial rapid decay as direct excitation processes cease followed by a peak due to repopulation of the n^3D levels by recombination. This conclusion was further confirmed through investigation of the pressure, current and quantum number (n) dependence of the afterglow radiation. Also, as the intensity peak was found to be proportional to $(\text{current})^3$ recombination was thought to proceed via the three body process. However, when the experiments were replicated in the He-Cd mixture no similar evidence for recombination was observed. This could only be explained if the Duffendak (thermal energy charge transfer) type process, i.e.

$$He^+(1^1S_0) + Cd(1^1S_0) \longrightarrow He(1^1S_0) + (Cd^+)^* + e$$

was more probable. While calculations did not support this conclusion, due either to restricted knowledge of the collision cross section or to an overestimate of the recombination rate coefficient, the experimental evidence was conclusive. Thus, we concluded that recombination does not provide a significant pathway for production of He (2^3S) species in the afterglow.

The role of collisional de-excitation of the higher lying helium levels in populating the metastable level was harder to assess. Using the semi-empirical cross section data of Fujimoto (1978) it was calculated that the rate coefficient for conversion of the 2^3P and 2^1P levels to the 2^3S level was of a similar order of magnitude to that of singlet to triplet conversion. Also, the 2^3P level is optically

connected to 2^3S with a lifetime of ∿40 nsec. As the steady state densities of the 2^3P, 2^1P and 2^1S levels were measured to be a significant fraction of the 2^3S density, rapid conversion of the former to the latter would give rise to a large metastable production term in the early afterglow.

Using the semi-empirical cross section data of Fujimoto (1978) and an assumed Maxwellian velocity distribution in the afterglow it was also shown that collisional de-excitation of the metastable species (to the ground state) was of the same magnitude as that for metastable destruction by Penning collisions in the early afterglow.

8.3.5 Model of Processes in the Afterglow

From the studies presented in Chapters 4, 5 and 6 a detailed picture of the afterglow emerged. In the early afterglow, the He (2^3S) level is populated via conversion of the higher lying levels either by electron collisions or radiative decay. Further, electronic de-excitation of the 2^3S level is significant, rivalling that of destruction by Penning collisions. Late in the afterglow the electronic production and loss terms become less significant and the decay is determined solely by Penning collisions and diffusion. Thus we would expect an initial density increase, the magnitude of which depends upon the relative populations of the higher lying levels, followed by a period of rapid decay, where the decay is determined by Penning collisions and electronic deactivation, giving way to an exponential tail in the late afterglow. These plausible changes in the 2^3S population are consistent with all the observed features of the 4416 Å decay in the afterglow, thus leading to

the conclusion that the Penning process alone is sufficient to account for excitation of the $5s^2\ ^2D_{5/2}$ level of Cd II.

This qualitative description was supported by a simplified set of rate equations describing the afterglow which were developed in Chapter 7 and incorporated the collision processes discussed in the previous three chapters. These rate equations were solved using a computer based numerical integration procedure together with the steady state excited helium and cadmium ion ground state densities derived in Chapter 3, estimates for the electron density, temperature and velocity distribution function and the available cross sections. Results of this calculation showed that the temporal dependence of the metastable density correlated closely with that of the measured 4416 Å decay. As further confirmation of the proposed model the current, pressure and cadmium concentration dependence of the 4416 Å decay were also replicated.

The current dependence of the relative peak height was explained by the fact that the population density of the 2^3S level increases relative to the 2^1S, 2^3P and 2^1P levels and thus conversion of the latter to the former will result in a smaller overall 2^3S density increase. At a constant current, the relative populations of all the helium levels remained essentially constant with increasing pressure and consequently the relative peak height is independent of pressure. The current and pressure dependence of the extrapolated exponential tail with the T=0 axis was explained by the increasing importance of electronic de-excitation of the 2^3S level as the electron density and hence collision rate is an increasing function of these two discharge parameters.

Thus, the 4416 Å spontaneous emission decay was explained solely in terms of the Penning collision mechanism populating the $5s^2\ ^2D_{5/2}$ level in the afterglow. No evidence was found which suggested that electronic

excitation of this level was significant and thus these results added further support to the earlier conclusion that the Penning collision mechanism is the dominant, if not sole, process by which the $5s^2\ ^2D_{5/2}$ level of Cd II is populated under the conditions which applied in the present discharge tube.

8.4 SIGNIFICANCE OF THE PRESENT RESULT

In this study the mechanisms leading to the excitation of the Cd II $5s^2\ ^2D_{5/2}$ upper level of the 4416 Å laser transition have been investigated. Because of the diverse practical applications of this type of metal vapour laser it is essential that the discharge kinetics are fully understood in order that the full potential of these devices is achieved. Of particular importance is the output power saturation with discharge current which has been reported by previous investigators.

Studies of both the d.c. discharge and corresponding afterglow were undertaken. From the study of the d.c. discharge it was concluded that the Penning collision mechanism alone is responsible for exciting the $5s^2\ ^2D_{5/2}$ level. While the afterglow was more complicated than anticipated, the conclusions drawn from the afterglow studies reinforced the view of the dominance of the Penning collision mechanism in these discharge types. In both these studies no clear evidence was found to suggest that electronic excitation of the $5s^2\ ^2D_{5/2}$ level has a significant role in populating this level.

From the present study we have thus concluded that the upper level of the 4416 Å transition is pumped predominantly by Penning ionization collisions. Since the He (2^3S) metastable density was observed to

saturate with current, this result apparently places a fundamental limit on the laser power output obtainable from these devices. Thus the laser power saturation observed in these lasers is a fundamental phenomenon and it is unlikely that output powers, of say 1 watt, will be achieved with this class of metal vapour laser.

Some increase in output power of these devices could be achieved by reducing the cathode bore diameter and consequently increasing the electron, ion and excited state densities. However, as the active volume is also reduced this will offset somewhat the increases in the excited state densities.

8.5 ASPECTS REQUIRING FURTHER INVESTIGATION

In this study only the collision mechanisms leading to the formation of the upper level of the blue 4416 Å laser transition have been investigated. In order to fully understand this system and, in particular, the reasons for the laser power saturation with current and pressure, the lower laser level (the $5p\ ^2P_{3/2}$ level) needs also to be subject to the same rigorous investigation.

As the main interest in this class of metal vapour laser lies in its potential as a source of coherent white light, the other laser transitions at 5337 Å, 5378 Å, 6355 Å and 6360 Å must also be more thoroughly investigated. In particular, excitation mechanisms of these levels and their dependence on the discharge parameters of current, helium pressure and cadmium concentration need to be firmly established.